

Fabrication of Microstructured Optical Fibres

Part I: Problem Formulation and Numerical Modelling of Transient Draw Process

S.C. Xue, R.I. Tanner, G.W. Barton, R. Lwin, M.C.J. Large and L. Poladian

Abstract — Microstructured optical fibres (MOFs) achieve their desired performance via a pattern of holes that run along the length of the fibre. Varying the hole pattern allows a variety of optical effects to be produced. However the original hole pattern within the preform may not be accurately transferred to the finished fibre due to the combined impact of material properties and the drawing conditions experienced during fabrication. In this two part paper, the processes of drawing MOFs having arbitrary cross-sectional hole structures will be analyzed for the case of Newtonian materials.

Part I presents a modelling formalism to describe the drawing processes, followed by a scaling analysis on a representative case, i.e. the non-isothermal drawing of an axisymmetric annular hollow fibre, to reveal the major factors influencing the drawing of both silica and polymer MOFs. By treating the primary draw process (i.e. from preform to intermediate cane) in fabricating polymer MOFs as a transient, isothermal problem, numerical simulations were carried out for an illustrative five hole structure. The results revealed the central importance of any steep neck-down region on hole shape deformation as well as the importance of forces additional to those associated with surface tension effects. Both experimental observations and numerical modelling show that a diversity of hole ‘activities’ (both in a hole’s relative size and shape) can occur when drawing MOFs.

Part II will extend both the analysis and numerical modelling with a focus on the steady-state continuous draw process (i.e. from preform or cane to fibre). In parallel with this analysis, we also present experimental results for the drawing of polymethylmethacrylate (PMMA) MOFs.

I. INTRODUCTION

MICROSTRUCTURED optical fibres have attracted increasing interest since they were first developed in the mid-

Manuscript received September 3, 2004. This work was financially supported by both the Australia Research Council and Cactus Fiber Pty Ltd. This support is gratefully acknowledged. All authors are from the University of Sydney, NSW 2006, Australia.

S. C. Xue and R. I. Tanner are with the School of Aerospace, Mechanical and Mechatronic Engineering, (email: shicheng@aeromech.usyd.edu.au; rit@aeromech.usyd.edu.au).

G. W. Barton and R. Lwin are with the Department of Chemical Engineering, (e-mail: barton@chem.eng.usyd.edu.au; R.Lwin@ofc.usyd.edu.au).

M. C. J. Large is with the Optical Fibre Technology Centre, (e-mail: M.Large@ofc.usyd.edu.au).

L. Poladian is with the School of Mathematics and Statistics, (e-mail: l.poladian@maths.usyd.edu.au).

1990’s [1,2]. Much of this interest is due to the fact that a wide variety of optical effects can be achieved by designing an appropriate hole pattern for the final fibre. For example, the hole pattern that gives rise to a graded refractive index fibre is shown in Fig. 1. These novel fibres have enormous potential in a diversity of applications from high-bandwidth, short-haul telecommunications to precision sensing in astronomy.

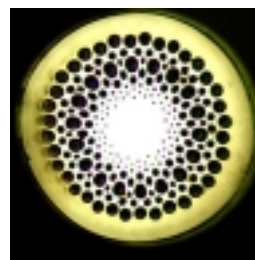


Fig.1. An illustrative mPOF hole pattern.

Initially MOFs were fabricated from silica, although more recently several research groups have succeeded in developing microstructured polymer optical fibres (mPOFs) [3,4,5]. The polymer most commonly used to date for mPOFs has been polymethylmethacrylate (PMMA). As the design/fabrication of mPOFs is currently more flexible than that for silica MOFs, the former are being extensively researched as a low cost option for a number of applications.

However from a manufacturing point of view, maintaining a cross-sectional hole pattern within an mPOF after the preform’s substantial extensional deformation within a non-isothermal environment can be difficult. Indeed it has been experimentally observed [6,7] that a range of hole deformation modes, affecting both a hole’s relative size and shape, can occur in drawing mPOFs. Such deformation may lead to a significant alteration of the fibre’s optical properties relative to the initial design, although there are occasions where hole deformation has been used to advantage. For example, Issa *et al.* [8] used controlled deformation as a means of generating the elliptical holes necessary for creating birefringent fibres. By contrast, in photonic band-gap fibres, whose structure generally involves holes of quite different diameters in close proximity, hole deformation can result in the desired optical function being lost completely. As a result, hole deformation needs to be understood to the level where it is either minimised (or compensated for) by designing appropriate preforms to

obtain the desired structure in the final fibre.

The complex deformation resulting from the drawdown process, either at the individual hole level or for the entire hole structure, is the result of the interactions between material properties (such as surface tension and temperature/stretch rate dependent viscosity), the drawing conditions (such as the thermal conditions within the draw zone and the draw tension), and of course the hole structure employed. A full understanding of these interactions is the long-term aim of this research.

From a theoretical point of view, it is not feasible to seek analytical solutions able to predict the deformation caused by these interactions when fabricating MOFs having arbitrary hole structures. Certainly in the case of mPOFs (that currently employ a two-stage drawing process, i.e the primary draw stage to take a preform to an intermediate cane; and the secondary draw stage to take this cane to final fibre [3, 4, 27]), a full mathematical analysis requires a description of processes that are combinations of non-isothermal, three-dimensional and time-dependent in nature. Any analytical approach is further complicated for mPOFs as the materials used have complex nonlinear viscoelastic behaviour meaning that rheological properties have to be considered.

Existing fibre drawing analyses [9-12] from the textile industry for modelling the spinning of molten threadlines cannot be directly applied to MOF drawing without major modifications. The most relevant recent literature is that of Fitt *et al.* [13-14] who used an asymptotic analysis to examine the behaviour of an annular glass hollow fibre. However their analysis gives no insight into either the possible hole deformation if a hole is eccentrically located, nor the interaction between holes within an overall structure during drawing MOFs. Such cases cannot be handled within the quasi-one-dimensional [9-14] analysis used by these authors.

As a first step towards a general description of the deformations affecting a MOF hole structure during drawing, Xue *et al.* [15] have recently studied the steady-state, isothermal drawing of a Newtonian material fibre containing a single hole. The likely impact of surface tension forces and internal pressurization on hole size changes was theoretically investigated for the case of a centrally located hole. They also demonstrated that for an asymmetrically located hole, the drawing process causes the original circular hole shape to become ovoid with the major axis being in the circumferential direction. However this analysis was concerned with relatively simple cases in which a single hole is involved. For analysing the drawing of MOFs with arbitrary hole structures, it seems certain that a numerical simulation approach will be necessary.

Such numerical modelling is a major challenge as the computational domain involves a number (possibly a quite large number) of substantially deformed three-dimensional free surfaces. To the best of our knowledge, such work has never been done comprehensively even for fibres made from Newtonian materials. Indeed only two reported numerical studies seem relevant to manufacturing MOFs. Lyytikäinen *et*

al. [16] looked at the impact of the hole structure on the time dependent heating behaviour of a PMMA preform, while Deflandre [17] investigated thermal effects on the periodicity and hole shape in the steady-state drawing process. All other numerical studies on the fibre drawing process have been limited in some way - either in terms of being for solid fibre with a temperature-dependent viscosity [18-22], for simple annular hollow fibre drawing processes in which the material is Newtonian [23-24], or else for solid fibre drawing processes with an assumed neck-down shape [25-26]. More importantly than their obvious limitations however, these studies make no real effort to assess the relative impact that viscous, inertial, gravitational and surface tension forces have on the drawing process. Thus the present work has three main aims. Firstly to present a modelling formalism that is appropriate to the MOF drawing problem. Secondly to carry out a scaling analysis on the governing system of equations for the general draw process to ascertain the relative importance of the various forces and mechanisms. Lastly we use the insights gained to begin the process of numerical modelling by carrying out a three-dimensional transient simulation of the primary draw stage for an mPOF structure containing five holes.

II. MODELLING FORMALISM FOR DRAWING MOFS

A. Process Description

The primary draw stage used in producing mPOFs is a transient process akin to tapering while the secondary draw stage is a continuous process. Note that silica MOFs are generally made using a single continuous draw. This paper focuses on the primary draw stage, while secondary drawing is considered in detail in Part II. However some aspects of the secondary draw process will be described in this paper, as the scaling analysis to be introduced can be applied equally to both transient and steady-state cases.

In the primary draw, a cylindrical polymeric preform of initial radius R_i and length L_i (shown schematically in Fig. 2 as containing just a single centrally located hole) is placed within an enclosed furnace. Once the temperature of the preform reaches the glass transition temperature, it begins to extend under its own weight (although in practice a certain amount of external force may also be applied) until the central portion achieves the required dimensions (typically about 10 mm in diameter). After cooling, this intermediate cane is then drawn to fibre in a continuous secondary draw.

Fig. 3 shows a schematic representation of the secondary draw process (again only showing a fibre containing a single central hole). Here the intermediate cane (for mPOFs) or the original preform (for silica MOFs) of initial radius R_i is fed into the preheating section of the draw tower at a feed speed V_i , then passed through the drawing section where it is heated above the glass transition temperature T_g (for polymer) or the softening point T_s (for silica) in a cylindrical furnace of length L . Fibre (with radius R_f) is continuously drawn from the end of the softened cane or preform by applying an appropriate

level of draw tension. The fibre diameter can be determined from mass conservation and the specified draw ratio D_r , defined as $D_r = V_f / V_i$ with $V_f (> V_i)$ being the draw speed.

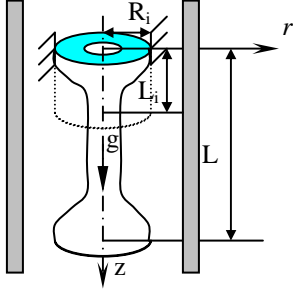


Fig. 2. Schematic diagram of the transient (primary) draw process for mPOF cane preparation.

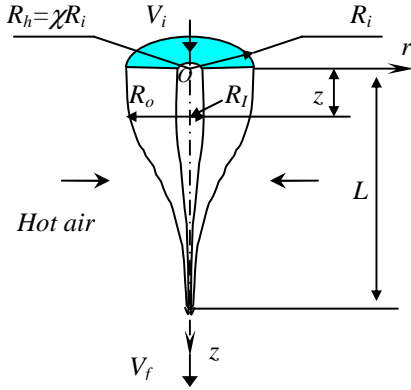


Fig. 3. Schematic diagram of a continuous draw process.

Note again that for silica MOFs, the preform (which may comprise a set of stacked capillaries) is typically drawn to fibre directly in this single-stage process. In Table I, we list the typical drawing conditions for PMMA and silica MOFs where T_w is the wall temperature of the heating furnace (for silica) or the hot air temperature (for the secondary drawing of an mPOF).

Table I
Typical MOF Drawing Conditions

Parameters	PMMA fibre	Silica fibre
R_i (mm)	5	12.5
R_f (mm)	240×10^{-3}	62.5×10^{-3}
T_w (°C)	220	2000
L (mm)	40-50	40-50
V_i (mm/min)	2.3	3.0
V_f (m/min)	1.0	120

Note that in our current experimental rig, convective heat transfer using hot air is used to heat the preform or cane. However we must stress here that radiative transfer may be the dominant heating mode in some cases, such as the drawing of silica MOFs.

The two draw stages are quite different. In the primary draw, deformation is mainly driven by gravity. Also deformation can only occur ‘properly’ when the temperature of the whole preform is above the glass transition temperature (and as close to uniform as possible). Hence the primary draw stage is a transient, but essentially isothermal process. By comparison, the secondary draw is a continuous process and hence once the final fibre is dynamically stable at the target diameter, the field variables should not change with time. However temperature gradients in both the radial and drawing directions are expected. Hence this draw process can be treated as a steady-state but non-isothermal problem. The analysis and modelling approaches for the two cases are thus inherently different.

B. Governing System of Equations

In general, any fibre fabrication process can be considered as a laminar transient or steady-state flow of an incompressible material. The basic equations governing such a flow comprise the following [9] – noting that here the Cartesian notation is used, where a sum is taken over repeated indices unless the contrary is stated:

- 1) mass conservation:

$$\frac{\partial v_k}{\partial x_k} = 0, \quad (1)$$

- 2) momentum conservation:

$$\rho \frac{\partial v_i}{\partial t} = \frac{\partial \sigma_{ik}}{\partial x_k} + \rho \left(f_i - v_k \frac{\partial v_i}{\partial x_k} \right) \quad (2)$$

- 3) energy conservation:

$$\rho c_p \left(\frac{\partial T}{\partial t} + v_k \frac{\partial T}{\partial x_k} \right) = \kappa \frac{\partial^2 T}{\partial x_k \partial x_k} + \phi + \nabla \cdot q_r, \quad (3)$$

Here v_k is the velocity vector, x_k is the coordinate vector, ρ is the density, t is time, and σ_{ij} is the Cauchy stress tensor given by $\sigma_{ij} = -p\delta_{ij} + \tau_{ij}$ with p being the isotropic pressure, δ_{ij} the Kronecker delta, and τ_{ij} the extra stress tensor (related to the flowing material’s kinematic quantities by an appropriate constitutive equation). In the ensuing scaling analysis and numerical simulations, we further assume that the material’s rheological behaviour is Newtonian in nature, and thus we have a linear constitutive equation

$$\tau_{ij} = \eta \left(\frac{\partial v_j}{\partial x_i} + \frac{\partial v_i}{\partial x_j} \right) \quad (4)$$

where η is the viscosity. For mPOFs, an appropriate nonlinear

viscoelastic model (see [9] for example) will be used in the next stage of our research.

In the momentum equations, the body force ρf_i is non-zero only for the component in the direction of the gravitational force. In the energy equation, T is the temperature, while c_p and κ are the heat capacity and thermal conductivity, respectively. The viscous dissipation function ϕ is given by

$$\phi = \tau_{ij} d_{ij} = \tau_{ij} \frac{\partial v_i}{\partial x_j}, \quad (5)$$

while $\nabla \cdot q_r$ denotes the divergence of the radiative heat flux (i.e. the radiative source term). For most materials, this term is non-zero because a body emits and absorbs energy at different wavelengths. When drawing fibres, radiation can be an important heat transfer mode, indeed dominating in the case of drawing silica MOFs. Therefore inclusion of thermal radiation can be critical for accurate predictions when modelling the temperature field within the extending preform. However an accurate description of radiative heat transfer needs to account for the spectrally dependent properties of the material. As the current work will (i) focus on which force terms are influential and thus should be included when modelling the MOF draw processes, and (ii) the numerical simulations that follow relate to drawing mPOFs within our current fabrication facility (where convective rather than radiative heat transfer is known to dominate), we will not consider radiative heat transfer further here (i.e. $q_r = 0$), other than to acknowledge its undoubted importance in modelling the drawing of silica MOFs.

C. Initial and Boundary Conditions

To fully specify any numerical description, it is necessary to impose appropriate kinematic and dynamic as well as thermal (for non-isothermal simulations) boundary conditions. In addition, the appropriate initial conditions for any transient process must be supplied. Obviously a quiescent velocity field over the entire computational domain can be reasonably imposed as the initial conditions for the primary draw stage. To specify all necessary boundary conditions, the cylindrical coordinate system is used here with the origin being placed at the centre of the top plane ($z = 0$).

At the top plane of the draw zone, the axial velocity is either zero (for the primary draw), or constant and equal to the feed speed V_i (for the secondary draw). At the bottom plane of the draw zone ($z = L$), a constant draw speed V_f (for the secondary draw) or axial tension force (if applied) is imposed.

At the air-solid interfaces over the entire length of the extending preform or cane ($0 < z \leq L$), deformation yields an outer ('neck-down' shape) free surface as well as a free surface within each internal hole. If the spatial position of a free surface $R(z, \theta, t)$ is described by a smooth function of the form $f(r, \theta, z, t) = R(\theta, z, t) - r$, then the appropriate kinematic boundary condition for the free surface should be:

$$\frac{Df}{Dt} = \frac{df}{dt} + v_i \frac{\partial f}{\partial x_i} = 0. \quad (6)$$

In addition to these kinematic boundary conditions, the dynamic boundary conditions should reflect the force balances pertaining to these free surfaces. In any fibre drawing process, it is generally assumed that there is no tangential force (i.e. zero shearing), although the relevant surface tension variations may have a role under some conditions (particularly when the fibre is drawn to a very thin diameter). Thus in general the force balance on a free surface will be expressed as,

$$\sigma_{ij} n_j s_i = 0, \text{ and } \sigma_{ij} n_j n_i = \pm K \sigma, \quad (7)$$

where n_i and s_i denote unit vectors normal and tangential to the surface, respectively. σ is the surface tension coefficient of the material used, while K is the sum of the principal curvatures of the free surface. A plus sign (+) applies for the inner hole surface, and a minus sign (-) for the outer fibre surface.

For non-isothermal secondary drawing situations, at the top plane, a temperature somewhat below T_g or T_s brought about by preheating of the polymer cane or silica preform is typically imposed. This boundary condition can be a function of position if the preform or cane has undergone asymmetric preheating. At the bottom plane of the draw zone, either the temperature profile across the fibre or the axial temperature gradient should be imposed.

In all cases the thermal conditions on the fibre outer surface are set via the local heat flux,

$$\kappa \frac{\partial T}{\partial n} = -h[T - T_a(z)] \quad (8)$$

where T_a is the temperature of the heat source within the draw furnace and h is the effective heat transfer coefficient.

D. Material Properties and Operational Conditions

Due to the wide variation in temperature during continuous fibre drawing, a temperature-dependent function should really be used for each material property (such as η , ρ , κ and c_p) for accurate predictions. This is particularly true for the viscosity which may vary by several orders of magnitude over the temperature range experienced during the preheating and drawing processes. However for the scaling analyses and illustrative numerical simulations in this study, only the temperature dependence of the viscosity is considered, with all other material properties taken as constant values at an appropriate reference temperature T_{ref} . Here we assume that viscosity obeys an Arrhenius type dependency

$$\eta(T) = \mu(T_{ref}) \exp \left[\frac{\Delta H}{R_g} \left(\frac{1}{T} - \frac{1}{T_{ref}} \right) \right], \quad (9)$$

where ΔH and R_g are the activation energy and the universal

gas constant, respectively, while μ is the viscosity at T_{ref} .

Table II
Representative Material Properties and Drawing Conditions

Property	PMMA	Silica	Units
Density (ρ)	1195	2200	kg/m ³
Viscosity (μ)	1.5×10^5	8.3×10^6	Pa.s
Surface tension coefficient (σ)	0.032	0.3	N/m
Thermal conductivity (κ)	0.2	2.68	W/m.K
Heat capacity (c_p)	1465	1345	J/kg.K
Activity energy ratio ($\Delta H/R_g$)	3218	6.1×10^4	K
Reference temperature (T_{ref})	443	1900	K
Glass transition (PMMA) or softening temperature (silica)	423	1900	K

In Table II, the material properties of PMMA and silica are listed. For PMMA, the surface tension coefficient measured by Wu [28] is used with other material properties as given by Reeve et al [22, 29]. For silica, the softening point of 1900 K is used as the reference temperature while the viscosity at this temperature is calculated from the relationship given by Bansal and Doremus [30]. The ratio $\Delta H/R_g$ is calculated from data given by Myers [19].

For continuous draw processes, the effective heat transfer coefficient h will be a function of the axial position z due to variations in both diameter and axial velocity. For example, in the case where PMMA cane is being drawn in our existing drawing facility, external heat transfer was described by two heat transfer coefficients. In the upper portion of the neck-down region where the cane diameter is essentially constant and the cane is moving slowly (essentially at its feed rate), an estimated value for h of 7.6 W/m²K was determined based on local gas flow conditions within the furnace. In the lower portion of the neck-down region where the fibre diameter is getting smaller and the fibre velocity is increasing, the effective heat transfer may be reasonably estimated by a correlation from Patel et al. [31],

$$h = 128.27V^{0.574} \quad \text{W/m}^2\text{K}, \quad (10)$$

where V is the local axial velocity of the fibre. Using this correlation gave an estimated value for h (under typical operating conditions) of 13.6 W/m²K.

For the operational conditions listed in Table I when drawing silica fibres, V falls in the range 0.05 to 2 m/s. Hence h varies from 23 W/m²K (in the upper part of the neck-down region) to 191 W/m²K (in the lower part).

III. SCALING ANALYSIS OF NON-ISOTHERMAL PROCESSES

In practice the full governing system of equations has to be solved numerically (subject to the appropriate initial and boundary conditions) if no further assumptions or

simplifications are made. However the computational load can be reduced and the numerical analysis more oriented with the reality of drawing if the less influential terms are removed from the system of equations. This relative ranking of terms for any complex hole structure can be provided by carrying out a ‘scaling analysis’ on the representative case, that is, the non-isothermal drawing of an axisymmetric annular fibre.

Following Schultz and Davis [11] - also see [15] - we use R_i to scale the radial distance, the length of the deformation zone L for the axial distance, V_i for the axial velocity while the quantity $V_i \frac{R_i}{L}$ for the radial velocity, the quantity L/V_i for time, T_{ref} for the temperature. The pressure and all stresses are scaled via the quantity $\mu \frac{V_i}{L}$. After scaling and assuming that

all material properties (except for the viscosity) are constant, the dimensionless form of the governing equations under a cylindrical coordinate system is as follows:

$$\frac{\partial u}{\partial r} + \frac{u}{r} + \frac{\partial w}{\partial z} = 0, \quad (11)$$

$$\begin{aligned} \varepsilon \text{Re} \left(\frac{\partial u}{\partial t} + u \frac{\partial u}{\partial r} + w \frac{\partial u}{\partial z} \right) = -\frac{\partial p}{\partial r} + \eta \left(\frac{\partial^2 u}{\partial r^2} + \frac{1}{r} \frac{\partial u}{\partial r} - \frac{u}{r^2} + \varepsilon^2 \frac{\partial^2 u}{\partial z^2} \right) \\ + 2\varepsilon \frac{\partial \eta}{\partial r} \frac{\partial u}{\partial r} + \frac{\partial \eta}{\partial z} \left(\varepsilon^2 \frac{\partial u}{\partial z} + \frac{\partial w}{\partial r} \right), \end{aligned} \quad (12)$$

$$\begin{aligned} \varepsilon \text{Re} \left(\frac{\partial w}{\partial t} + u \frac{\partial w}{\partial r} + w \frac{\partial w}{\partial z} \right) = -\varepsilon^2 \frac{\partial p}{\partial z} + \eta \left(\frac{\partial^2 w}{\partial r^2} + \frac{1}{r} \frac{\partial w}{\partial r} + \varepsilon^2 \frac{\partial^2 w}{\partial z^2} \right) \\ + 2\varepsilon^2 \frac{\partial \eta}{\partial z} \frac{\partial w}{\partial z} + \frac{\partial \eta}{\partial r} \left(\varepsilon^2 \frac{\partial u}{\partial z} + \frac{\partial w}{\partial r} \right) + \frac{\text{Re}}{Fr}, \end{aligned} \quad (13)$$

$$\varepsilon P_e \left(\frac{\partial T}{\partial t} + u \frac{\partial T}{\partial r} + w \frac{\partial T}{\partial z} \right) = \frac{\partial}{\partial r} \left(r \frac{\partial T}{\partial r} \right) + \varepsilon^2 \frac{\partial}{\partial z} \left(\frac{\partial T}{\partial z} \right) + \varepsilon^2 B_r \phi, \quad (14)$$

where u and w are respectively the radial and axial velocities. Note that here, the viscosity η has been scaled by μ .

The kinematic, dynamic and thermal boundary conditions previously described by Eqs. 6-8 now become:

$$u = \frac{\partial R}{\partial t} + w \frac{\partial R}{\partial z}, \quad (15)$$

$$2\varepsilon^2 R' \left(\frac{\partial u}{\partial r} - \frac{\partial w}{\partial z} \right) + (1 - \varepsilon^2 R'^2) \left(\varepsilon^2 \frac{\partial u}{\partial z} + \frac{\partial w}{\partial r} \right) = 0 \quad (16)$$

$$\begin{aligned} p \left(1 + \varepsilon^2 R'^2 \right) - 2\eta \left[\frac{\partial u}{\partial r} + \varepsilon^2 R'^2 \frac{\partial w}{\partial z} + R' \left(\varepsilon^2 \frac{\partial u}{\partial z} + \frac{\partial w}{\partial r} \right) \right] \\ = \mp \frac{1}{\varepsilon C_a} \left\{ \frac{1}{R} \left(1 + \varepsilon^2 R'^2 \right)^{\frac{1}{2}} - \varepsilon^2 R'' \left(1 - \varepsilon^2 R'^2 \right)^{-\frac{1}{2}} \right\}, \end{aligned} \quad (17)$$

$$\frac{\partial T}{\partial n} = -B_i [T - T_a(z)], \quad (18)$$

where $R' \equiv \partial R / \partial z$ is the slope of a free surface.

A series of dimensionless numbers arise from this scaling of the governing equations including: aspect ratio $\varepsilon = R_i/L$ ('slenderness' of the extending preform or cane); Reynolds number $R_e = \rho V_i R_i / \mu$ (ratio of inertial and viscous forces); Froude number $F_r = V_i^2 / g R_i$ (ratio of inertial and gravitational forces); Peclet number $P_e = \rho c_p V_i R_i / \kappa$ (ratio of convective heat transfer to conductive heat transfer; Brinkman number $B_r = \mu V_i^2 / \kappa T_{ref}$ (ratio of heat production by mechanical dissipation to heat transfer by conduction); Capillary number $C_a = \mu V_i / \sigma$ (ratio of viscous and surface tension forces); and Biot number $B_i = h R_i / \kappa$ (ratio of the internal and external resistances to heat transfer in the radial direction).

If the extending preform or cane can be characterized as a 'slender body' (i.e. $\varepsilon \ll 1$), then the leading order (in terms of ε) system of scaled equations for steady-state drawing processes can be readily obtained. The deformation process can be characterized as a quasi one-dimensional (all variables are independent of the radial position) extensional flow, and the axial fibre velocity profile w can be cast as (see [32] for example) a simple function of the draw ratio and position z :

$$w = D_r^z \quad (19)$$

The variations of R_o and R_I in the drawing direction can be expressed as a coupled set of equations:

$$\frac{dR_o}{dz} = -\frac{1}{2w} \left[R_o \left(\frac{dw}{dz} \right) + \left(\frac{1}{\eta \varepsilon C_a} \right) \left(\frac{R_I}{R_o - R_I} \right) \right], \quad (20)$$

$$\frac{dR_I}{dz} = -\frac{1}{2w} \left[R_I \left(\frac{dw}{dz} \right) + \left(\frac{1}{\eta \varepsilon C_a} \right) \left(\frac{R_o}{R_o - R_I} \right) \right]. \quad (21)$$

For this leading order approximation, the impact of the thermal dependency of the viscosity on fibre drawing is only seen if surface tension effects are included in the model description. If the latter are not considered, then the fibre draw behaviour is indistinguishable from an isothermal case. Thus numerical simulation is required (as might have been expected) to handle the non-isothermal case.

However by examining the relative order of magnitude of the dimensionless numbers in the scaled equations under likely operational conditions, we can infer which forces (e.g. inertial, gravitational and surface tension) and mechanisms (e.g. convective heat transfer) will play a dominant role in different drawing processes. Such information also provides an insight into the most appropriate boundary conditions for any subsequent numerical calculations.

After estimating each dimensionless numbers at the primary drawing stage, we conclude that inertial force is always

negligible as εR_e is at most of order 10^{-10} , while the gravitational force cannot be neglected in the early stages as R_e/F_r is of order 10. Indeed this is the initial driving force for the preform 'flowing' and elongating. However in the later stages, this force becomes negligibly small and the elongation process has (in practice) to be aided by the application of an external draw tension. As far as surface tension is concerned, as the term $1/\varepsilon C_a R$ is of order $10^{-1}/R$ during the whole process, this force can be important as the dimensionless hole radius R (relative to R_i) is usually less than 10^{-1} particularly after significant elongation has occurred.

Following Xue *et al.* [15], a similar scaling analysis can be performed for a continuous, non-isothermal draw process (both for silica MOFs and mPOFs). Under typical operating conditions on our facility the draw ratio D_r is about 435 for PMMA fibres but may be considerably higher ($D_r = 4 \times 10^4$) for silica fibres. Estimated (order of magnitude) values for each dimensionless number lead to the following conclusions:

- Both inertial and gravitational forces are negligible in both PMMA and silica MOF cases as εR_e is never more than about 10^{-6} while R_e/F_r is never more than 10^{-8} .
- Surface tension can become important for both PMMA and silica MOF cases if the dimensionless radius of a hole relative to R_i reduces to even a modest value of 10^{-4} ratio.
- In the absence of radiative transfer, external heat transfer (by convection) in both cases leads to a large value for the term εP_e (i.e. of order 10^1 - 10^2). Such a value means that temperature gradients along the streamlines will be small and thus a zero temperature gradient boundary condition can be reasonably imposed at the exit to the draw zone.
- In both silica MOF and mPOF cases a negligible radial temperature gradient is expected as B_i is always less than 10^{-1} . However the fibre temperature at any point in the drawing process is expected to be sensitive to the external environment (i.e. to the temperature and flow fields around the fibre). This means that the thermal boundary conditions imposed at the external free surface will have a critical impact on both the development of the neck-down profile and the internal hole deformation.
- Mechanical dissipation can be safely ignored for mPOFs as $\varepsilon^2 B_r$ is well below 1 at the exit to the draw zone. However this effect cannot be ignored when drawing silica MOF as here $\varepsilon^2 B_r$ is of order 10 at the exit.

IV. NUMERICAL SIMULATIONS

A. Finite Element Solution Method

The previous scaling analyses allowed us to assess the likely impact of the various terms within the system of governing equations for fibre drawing processes. This guidance has been central to our approach to numerically modelling MOFs.

A commercial software package (Polyflow) based on finite

element methods has been used for our numerical simulations. The details of its features are documented elsewhere [33]. One of this package's most attractive features is its robust ability to remesh the computational domain by relocating internal nodes according to the displacement of boundary nodes. This is clearly a useful feature for fibre drawing where the gross dimensions of the system change considerably.

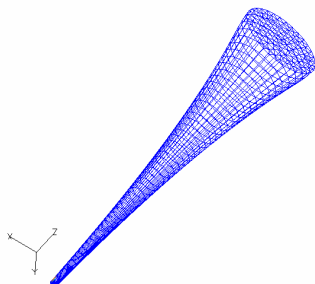


Fig. 4. Final computational domain and mesh structure.

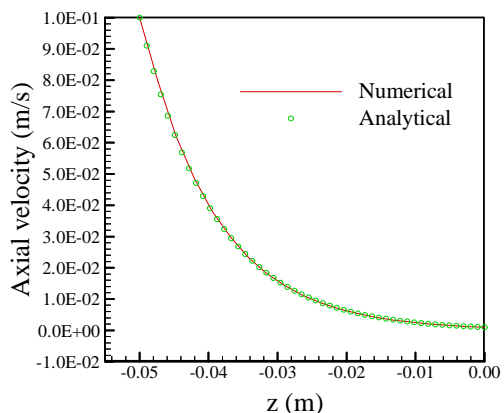


Fig. 5. Velocity profile along the centreline of solid fibre.

In this paper, we focus on simulating the transient, isothermal primary draw process used in fabricating mPOFs. In these preliminary simulations, PMMA is treated as Newtonian (in terms of its rheological flow behaviour). In Part II, the focus moves to steady-state, non-isothermal continuous draw processes.

B. Accuracy of POLYFLOW Based Modelling

To check the package's ability to handle flow problems involving dramatic free surface deformation, we began by considering a simple drawing process for which analytical solutions are available, that is, the drawing of an axisymmetric Newtonian solid fibre characterized by a small aspect ratio ϵ under steady-state, isothermal conditions.

A solid preform with R_i of 5 mm is fed into the drawing furnace at a speed of 1.0 mm/s and drawn down to fibre over a hot zone length $L = 50$ mm at a draw ratio D_r of 100. In view of the system symmetry, the domain was discretized as 10 uniform elements in the radial direction and 50 elements with gradually increasing step size in the drawing direction. The

radial discretization used irregular triangular meshes on the planes normal to the drawing direction. In this way, 10200 hexahedral volume elements were created by discretising the entire domain. Together with the relevant boundary conditions, the governing system of equations was solved using a coupled (Newton-Raphson) iterative scheme. The final calculated domain is shown in Fig. 4. No problems were encountered handling the large free surface deformation. Fig. 5 compares the known analytical solution for the centreline velocity profile (see Eq. (19)) with the numerical prediction. The agreement was more than satisfactory.

C. Polyflow Modelling of mPOF Primary Draw

Before this study, our experimental data on the nature and extent of hole deformation during the primary draw stage had been ambiguous. Thus we chose next to numerically model this process. Although it was realised from the previous scaling analysis that surface tension effects would likely have some impact, these were not included here to highlight the influence of other possible deforming forces.

The primary draw of a preform with $R_i = 35$ mm and $L_i = 80$ mm was numerically modelled. The original cross-sectional hole pattern in the preform is shown in Fig. 6 (where only half the symmetric domain is shown). A large hole with a dimensionless radius (normalised against R_i) $\chi=0.20$ is located at the centre with four smaller holes (for which $\chi=0.043$) symmetrically arranged around this central hole. The dimensionless spacing between the centres of the large and small holes is $\Delta=0.357$.

In practice, in order to hold the mPOF preform in place, its top end must be attached to a support. In order to mimic this experimental arrangement, a linearly decreasing viscosity was imposed within the simulation over the section $0 \leq Z \leq R_i/L_i$. Thus the PMMA viscosity gradually decreases to the value at the reference temperature (170°C) at the non-dimensional axial position $z = R_i/L_i = 0.4375$. This arrangement meant that major deformations to the preform (and its internal hole structure) started around there, instead of at the very top.

Examination of the hole structure at various cross-sections reveals that:

- Around the steep neck-down region, the shape of the smaller holes changes dramatically, being characterized by a move to an ovoid shape whose major axis is parallel to the surface of the larger central hole. That is, the hole with a larger curvature (i.e. the smaller hole) changes its shape so that the curvatures of the two adjacent holes tend to 'match' each other.
- Around the neck-down region, hole enlargement takes place. i.e. an increase in the absolute size of the hole.
- These hole 'activities' become less pronounced with increasing separation (in the axial direction) from the steep neck-down region.

To check that these predictions are not simply numerical artefacts, the simulations were repeated with various mesh refinement. The results were essentially indistinguishable

from each other. This is expected considering the material is linear, and the first order numerical accuracy in space can give good predictions

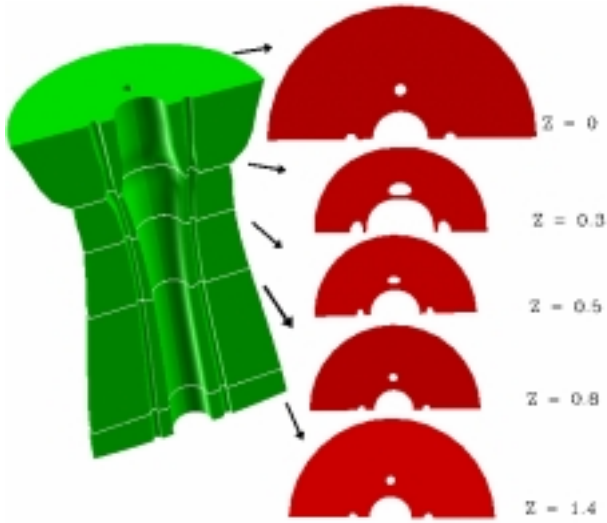


Fig. 6. Computed hole structure deformations at different cross-sections in the primary draw for mPOF.

The phenomenon of hole enlargement in the absence of pressurization during the draw-down process is counter-intuitive. It is though, confirmed by experimental observation, as shown later, in Fig. 7. To analytically explain this phenomenon is demanding due to its occurring in this transient and non-slender-body process. However by realizing that the primary draw is essentially a material redistribution process, this hole behaviour can be explained from a mass conservation perspective. As the preform starts extending, the axial velocity increases from zero to a maximum around the neck-down point (i.e. $Z = 0.3$ as shown in Fig. 6). To observe mass conservation, the net cross-sectional area has to decrease inversely with the increasing velocity. As a result not only does the external radius shrink to form the neck-down region, but the inner hole also undergoes enlargement in this vicinity. With this explanation, it is to be expected that the smaller the hole radius (relative to the preform radius) and the steeper the neck-down region (thus, the higher the acceleration in the extending axial velocity), the more pronounced hole enlargement will be.

With respect to hole shape changes, numerical simulations performed with the inclusion of surface tension effects have shown no discernible difference. Thus the predicted hole shape changes were not due to any difference in curvature dependence surface tension forces around different size holes.

In part II of this work, by performing localized force balance over a extending preform or cane, we will elucidate the driving forces responsible for changes in both hole size and shape with particular emphasis on continuous draw processes.

Finally, we must point out that hole behaviour is certainly important from a fabrication point of view. However hole deformation occurring during the primary drawing of mPOFs

need not necessarily be passed on to the secondary draw stage, as long as the intermediate cane is taken from that part of the extended preform well away from the steep neck-down region.

V. EXPERIMENTAL OBSERVATIONS

To confirm our numerical predictions on hole behaviour in the primary drawing of mPOF, a suite of experiments has been performed by drawing preforms made from commercial grade PMMA.



Fig. 7. Neck-down region of an extending PMMA preform containing a centrally located hole.

Firstly we considered preforms containing a single centrally located hole. Dimensionless hole sizes ranged from $\chi=0.25$ to 0.5. The neck-down region for the $\chi=0.25$ case is shown in Fig. 7. Note the clear hole enlargement that has occurred immediately below the fixed end in the region experiencing a sharp neck-down. As predicted numerically, the smaller the hole radius, the more pronounced the observed hole enlargement.

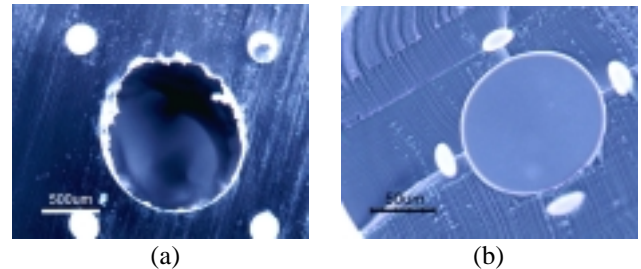


Fig.8. Cross-section of (a) the PMMA cane after the primary draw stage and (b) the mPOF after the secondary draw.

Drawing an mPOF preform having the same five hole structure as used in the numerical simulations was also carried out. The observations were in agreement with the simulations. A cross-section cut from the final cane well away from the steep neck-down region is shown in Fig. 8(a). Here the smaller holes have not dramatically changed their shape as a result of the primary draw process. For comparative purposes, Fig. 8(b) shows a cross-section cut from the finished fibre drawn down from the cane at a relatively high draw ratio ($D_r = 435$) in our secondary draw tower. Here dramatic changes in hole shape are in evidence, showing that deformation of small holes (from near circular to decidedly ovoid) when adjacent to a larger

hole occurs during this later draw stage.

VI. CONCLUSIONS

Microstructured optical fibres have enormous potential. The realisation of this potential is to some extent linked to the ability of the fabrication process employed to maintain the hole structure in the final fibre as close as possible to that designed. This paper has shown how scaling the governing system of equations allows a quantitative analysis to be made regarding the relative importance of the many interactions involving heat transfer, material rheological properties. The combination of scaling analysis and numerical modelling has demonstrated that while surface tension effects are certainly important in some cases, they are not the dominant mechanism in hole shape deformation. It is anticipated that this work will have an impact in the future on both the way MOFs are designed and the way they are fabricated.

Part II of this paper will focus on extending our analysis and numerical modelling to describe continuous draw processes.

REFERENCES

- [1] J. C. Knight, T. A. Birks, R. F. Russell and D. M. Atkins, "All silica single-mode optical fiber with photonic crystal cladding," *Opt. Lett.*, vol. 21, No. 19, pp. 1547-1549, 1996.
- [2] T.A., Birks, J.C., Knight, and P. St. J., Russell, "Endlessly single-mode photonic crystal fibre," *Opt. Lett.*, vol. 22, pp 961-963, 1997.
- [3] M. A. van Eijkelenborg, M. C. J. Large, A. Argyros, J. Zagari, S. Manos, N. A. Issa, I. Bassett, S. Fleming, R. C. McPhedran, C. M. de Sterke and N. A. P. Nicorovici, "Microstructured polymer optical fibre," *Opt. Exp.*, vol. 9, No. 7, pp.319-327, Sep. 2001.
- [4] M. A. van Eijkelenborg, A. Argyros, G. Barton, I. Bassett, M. Fellow, G. Henry, N. A. Issa, M. C. J. Large, S. Manos, W. Padden, L. Poladian and J. Zagari, "Recent progress in microstructured polymer optical fibre fabrication and characterisation," *Opt. Fiber Technol.*, vol. 9, pp.199-209, April. 2003.
- [5] J. Choi, D. Y. Kim, U.C. Peak, "Fabrication of properties of polymer photonic crystal fibre," in *Proc. Plastic Optical Fibre Conf.* Amsterdam, Sep. 2001, pp. 355-360.
- [6] M. Large, G. Barton, R. Lwin, L. Poladian, R. I. Tanner, S. C. Xue and H. Yu, "Hole Deformation in Microstructured Optical Fibres," 30th Euro. Conf. on Optical Communication, Sept. 2004, Stockholm, Sweden, Program number We4.P.034.
- [7] L. Poladian, G. Barton, M. Large, R. Lwin, W. Pok, R. I. Tanner, M. A. van Eijkelenborg and S.C. Xue, "Microstructured Polymer Optical Fibres: Impact of Imperfections in Design and Manufacture," OECC/COIN 2004, July, Yokohama.
- [8] N A Issa, M A van Eijkelenborg, G Henry, M Fellow, M C J Large, "Fabrication and characterization of microstructured optical fibres with elliptical holes," *Opt Lett*, vol. 29, pp. 1336-1338, 2004.
- [9] R.I Tanner, *Engineering Rheology*, (2nd Ed.), Oxford University Press Inc., New York, .2000, pp 340-356.
- [10] M. R. Matovich and J. R. A. Pearson, "Spinning a molten threadline-Steady-state isothermal viscous flows." *Ind. Eng. Chem. Fundam.*, vol. 8, pp. 512-520, 1969.
- [11] W. W. Schultz and S. H. Davis, "One-dimensional liquid fibers," *J. Rheol.* vol. 26, No. 4, pp. 331-345, 1982.
- [12] M. M. Denn, in: J. R. A. Pearson, S. M. Richardson (Eds.), *Computational Analysis of Polymer Processing*, Applied Science Publication, London, 1983, pp. 179-215.
- [13] A. D. Fitt, K. Furusawa, T. M. Monro and C. P. Please, "Modeling the fabrication of hollow fibers: capillary drawing." *J. Lightwave Technol.*, vol. 19, No. 12, pp.1924-1931. Dec. 2001.
- [14] A. D. Fitt, K. Furusawa, T. M. Monro, C. P. Please and D. J. Richardson, "The mathematical modeling of capillary for holey fibre manufacture." *J. Eng. Math.*, vol. 43, pp. 210-227. May, 2002.
- [15] S. C. Xue, R. I. Tanner, R. Lwin and G. Barton., "Drawing optical fibres containing holes," *ZAMP*, to be submitted, 2005.
- [16] K. Lytyikäinen, J. Zagari, G. Barton, J. Canning, "Heat transfer in a microstructured polymer optical fibre," *Modelling and Simulation in Materials Science and Engineering*, vol. 14, pp. 1-11, 2004.
- [17] G. Deflandre, "Modeling the manufacturing of complex optical fibres: the case of the holey fibres," in *Proc 2nd Int. Colloquium.*, Valenciennes, France, Jan. 2002, pp. 150-156.
- [18] U. C. Paek and R. B. Runk, "Physical behavior of the neck-down region during furnace drawing of silica fibres," *J. Appl. Phys.* vol. 49, pp. 4417-4422, August 1978.
- [19] M.R. Myers, "A model for unsteady analysis of preform drawing," *AIChE Journal*, vol. 35, pp. 592-602, 1989.
- [20] S. R. Choudhury and Y. Jaluria, "A computational method for generating the free-surface neck-down profile for glass flow in optical fibre drawing." *Numer. Heat Transfer*, Part A, vol. 35, pp. 1-24, 1999.
- [21] K. Lytyikäinen, P. Råback, and J. Ruokolainen, "Numerical simulation of a specialty optical fibre drawing process," in *Pro 4th Int ASME/JSME/KSME Symp on Computational Technologies for Fluid/Thermal/ Chemical/ Stress Systems with Industrial Applications*, Vancouver, BC, Canada, 2002, vol. PVP448-2, pp. 267-275.
- [22] H. M. Reeve, A. M. Mescher and A. F. Emery, "Steady-state heat transfer and draw force for POF manufacture." in *12th Int. Conf. on Polymer Optical Fibre*, Seattle, WA, Sep. 2003, pp. 220-223.
- [23] A. L. Yarin and P. Gospodinov and V. I. Roussinov, "Stability loss and sensitivity in hollow fibre drawing." *Phys. Fluids*, vol. 6, No. 4, pp. 1454-1463, April 1994.
- [24] P. Gospodinov and A. L. Yarin , "Draw resonance of optical microcapillaries in non-isothermal drawing." *Int. J. Multiphase Flow*, vol. 23, No.54, pp. 967-976, Feb. 1997.
- [25] S. H.-K. Lee, Y. Jaluria, "The effects of geometry and temperature variations on the radiative transport during optical fibre drawing." *J. Materials Processing & Manufacturing Sci.*, vol. 3, pp. 317-331, April 1995.
- [26] J. Liu, S. J. Zhang and Y. S. Chen, "Advanced simulation of optical fiber drawing process," *Numer. Heat Transfer*, Part A, vol. 40, pp. 473-495, 2001.
- [27] G. Barton, M. A. van Eijkelenborg, G. Henry, M. C. J. Large, J. Zagari, "Fabrication of microstructured polymer optical fibres," *Opt. Fiber Technol.*, vol. 10, pp. 325-335, May, 2004.
- [28] S. Wu, "Surface and interfacial tensions of polymer melts. II. Poly(methylmethacrylate), poly(n-butylmethacrylate), and polystyrene," *J. Phys. Chem.*, vol 74, pp. 632-638, 1970.
- [29] H. M. Reeve, A. M. Mescher and A. F. Emery, "Experimental and numerical investigation of polymer preform heating," *J. of Materials Processing & manufacturing Science*. vol. 9, pp. 285-301, 2001.
- [30] N. P. Bansal and R. H. Doremus, *Handbooks of Glass Properties*, Academic Press, New York, 1986. pp. 680.
- [31] R. M. Patel, J.H. Bheda, J. E. Spruiell, "Dynamics and structure development during high-speed melt spinning of Nylon 6. II. Mathematical modeling," *J. Appl.Polym.Sci.*, vol. 42 pp. 971-994, 1991.
- [32] A. Yarin, VI. Rusinov, P. Gospodinov, St. Radev, "Quasi one-dimensional model of drawing of glass microcapillaries and approximate solutions," *Theor. Appl. Mech.*, vol. 20, pp. 55-62, 1989.
- [33] POLYFLOW User's Manual, ver. 3.10, Fluent Inc. Centerra Resource Park, 10 Cavendish Court, Lebanon, NH 03766.USA, Sep. 2003.